

# Power System Fast Frequency Control in Low Inertia Environment Using MPC

Byungchul Kim<sup>a,1</sup> and Eyad H. Abed. <sup>a</sup>  
<sup>a</sup>University of Maryland at College Park

**Abstract.** Rapid development of renewable energy systems is causing considerable reduction of inertia and damping in the power system networks. This adds difficulty to frequency control. This paper suggests a novel method of frequency control for low inertia power systems using a model predictive control (MPC) loop with the goal of fast frequency response to offer quick frequency control to service areas. The controller manages the voltage source converter's power injections to ensure operation within the frequency limits and optimal power flow in the presence of power system's disturbances. Optimized MPC goal function methods are used for simulation verification and performance enhancement. An IEEE 39-bus system dynamic model is used to illustrate the effectiveness of the proposed control methods.

**Keywords.** Fast frequency control, low-inertia, model predictive control, virtual synchronous machines, centralized control.

## 1. Introduction

Large area electric energy generation employing inverters and voltage source converters brings about new problems in real-time power system operation and management. Reduced inertia and damping induce large-scale frequency deviations [1], [2]. To enhance the flexibility of a low-inertia system and alleviate possible stability problems, a new fast frequency control (FFC) ancillary service is needed [2]. This can be achieved through use of DC energy storage systems (ESS), and grid-forming voltage source inverters (VSIs) and voltage source converters (VSCs) by effectively modulating the output power in response to frequency fluctuations.

Grid-forming VSI/VSC control methods include virtual synchronous machines (VSM) modeled after the dynamics of a synchronous machine [3], and droop-based control which uses the converter's active and reactive power output and the droop control property [4]. However, most of the control methods focus only on the converter's AC side, neglecting the DC link dynamics. These approaches make the simplifying assumption that limited energy and power is available at the DC side capacitor [5]. Also, under a small frequency deviation, a constant droop gain causes unsatisfactory VSI/VSC performance. It hinders the inverter/converter from using maximum power capacity in response to disturbances and faults.

Model predictive control (MPC) is an online optimization-based control technique which combines all system constraints and the objective goal function into a unified

---

Corresponding Author, Byungchul Kim, University of Maryland, College Park, MD., USA; E-mail: victorykim0516@gmail.com

framework [6]. Using MPC, one can calculate optimal inputs based on predicted future state evolution using a state space representation of the system and incorporating constraints within the objective function. Due to these features, MPC is viewed as an appealing technique for controlling frequency in the power systems.

Recently, several papers have applied the MPC in centralized [7], distributed [8], and hierarchical [9] power system control, and it was found to yield better performances in the robust control of frequency and frequency uncertainty modulation in comparison with PI control. However, few publications have discussed using MPC in the fast frequency control [10]. In [10], real time optimal frequency and inertia response control was used with explicit MPC. However, that work did not demonstrate converter-based power generation, and used a simplified power system model for fast frequency control.

Disadvantages of MPC based frequency control in an HVDC grid were discussed in [11], [12]. Decentralized MPC-based frequency control has also been proposed as a measure to be applied in emergency situations to avoid triggering under frequency load shedding relays [11]. Based on measurement of rate-of-change-of-frequency (ROCOF), frequency predictions are created and the VSI/VSC output is updated when the frequency violations are anticipated or captured. Although decentralized, this method requires grid topology and HVDC converter locations to compute sensitivity factors connected to DC voltage drop. Increased computational burden in online solution of the MPC problem and tuning parameters are limitation of this method. A VSC based HVDC link furnished with a centralized MPC controller is promising for stabilization of large power systems [12]. VSC inputs are modulated to damp out oscillations in the power system using global measurements. However, communication delays and failures may potentially lead to stability problems. Reliable, and rapid communication links are necessary for the system to benefit from MPC.

We propose a centralized MPC based FFC methodology which can be integrated as an additional layer for simplified quadratic cost goal function calculation to the loop frequency control. In the event of large disturbances MPC keeps the frequency deviation and ROCOF within limits prescribed by the user. We begin by adjusting model identification techniques to estimate the parameters of the frequency response model based on measured data. Moreover, to improve in computational efficiency and reduce the computational burden, we propose a systematic centralized MPC method. Finally, the proposed control design is verified through time domain simulations for a low-inertia system within a large-scale power systems.

## **2. Voltage Source Converter Frequency Control**

### *2.1. MPC based VSG*

For the traditional virtual synchronous generator (VSG), frequency regulation is difficult to regain once it deviates from normal. Even if the frequency is steered back to normal under small inertia, the frequency may be forced to stabilize quickly which can possibly cause oscillations. Frequency regulation capability is difficult to enhance. Moreover, when frequency deviates from normal, the dynamic response of the system is expected to decelerate. Conversely, the system responds quickly when the post-disturbance frequency returns to normal [15]. Here, a MPC-based VSG control scheme is suggested to enhance accuracy of frequency control. Simple modeling of a VSG is illustrated in

Fig. 1. This provides inertia for stability support, voltage reference with reactive droop control, and power calculation with active droop control.

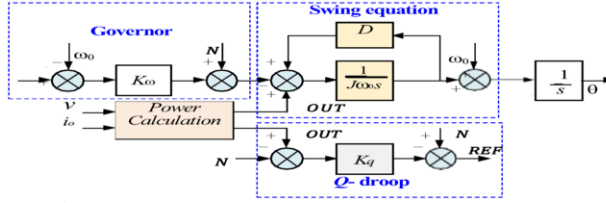


**Figure 1.** Illustrating simple model of voltage-controlled VSG.

Given a frequency variation, the major function of the governor part is to respond by appropriately managing the active power output. The Q-droop is used in output voltage control, since the reactive power is associated with AC bus voltage. The governor and Q-droop formulation result in a droop control technique written as

$$\begin{cases} P_{OUT} = P_N - K_\omega(\omega - \omega_0) \\ V_{REF} = V_N - K_q(Q_{OUT} - Q_N) \end{cases} \quad (1)$$

where  $P$  and  $\omega$  are virtual active power of the governor and generated angular frequency of the VSG, respectively. Also  $P_N$  and  $V_N$  are nominal active power and nominal voltage;  $K_\omega$  and  $K_q$  are frequency deviation gain and Q-droop coefficient;  $V_{REF}$  and  $Q_{OUT}$  are reference voltage and instantaneous output reactive power;  $\omega_0$  and  $Q_N$  are nominal angular frequency and nominal reactive power, respectively. The swing equation as the main part of the VSG, is included to emulate rotor inertia that would be provided by a synchronous generator (SG). The swing equation can be represented as

$$J\omega_0 \frac{d}{dt}(\omega - \omega_0) = P - P_{OUT} - D(\omega - \omega_0) \quad (2)$$

where  $J$ ,  $P_{OUT}$  and  $D$  are moments of virtual inertia, output power, and damping coefficient, respectively.

The discrete MPC model for the VSG is represented here to achieve efficient control during a sampling period. A discrete model can be obtained from Eq. (2) using Tustin approximation:

$$J\omega_0[\omega(k+1) - \omega(k)] = T_s[P(k) - P_{OUT}(k)] - T_s D[\omega(k) - \omega_0] \quad (3)$$

where  $T_s$  is the sampling interval.

An incremental discrete model can be obtained through algebraic manipulation of Eq. (3), yielding

$$\Delta \omega(k+1) = A_e \Delta \omega(k) + B_e \Delta P_{OUT}(k) + B_u \Delta P(k) \quad (4)$$

where  $A_e = 1 - \frac{T_s D}{j\omega_0}$ ,  $B_e = -\frac{T_s}{j\omega_0}$ ,  $B_u = \frac{T_s}{j\omega_0}$ .

The output follows the dynamics:

$$y(k+1) = y(k) + \Delta \omega(k+1) \quad (5)$$

Setting the prediction horizon as  $n$  steps, and assuming it takes  $l$  steps to reach steady state, then the output  $Y_n(k+1|k)$  can be represented as

$$Y_n(k+1|k) = l y(k) + S_x \Delta \omega(k) + S_u \Delta P(k) + S_e \Delta P_{OUT}(k) \quad (6)$$

where  $\mathbf{I} = [1 \ 1 \ \dots \ 1]_{1 \times n}^T$ ,  
 $\mathbf{P}(k) = [\Delta P(k) \ \Delta P(k+1) \ \dots \ \Delta P(k+l-1)]_{1 \times n}^T$ ,  
 $\mathbf{S}_x = \left[ A_e \ \sum_{i=1}^2 A_e^i \ \dots \ \sum_{i=1}^n A_e^i \right]_{1 \times n}^T$ ,  
 $\mathbf{S}_e = \left[ B_e \ \sum_{i=1}^2 A_e^{i-1} B_e \ \dots \ \sum_{i=1}^n A_e^{i-1} B_e \right]_{1 \times n}^T$ ,  
 $\mathbf{S}_u = \left[ \begin{array}{cccc} B_u & 0 & \dots & 0 \\ \sum_{i=1}^2 A_e^{i-1} B_u & B_u & \dots & 0 \\ \dots & \dots & \dots & 0 \\ \sum_{i=1}^n A_e^{i-1} B_u & \sum_{i=1}^{n-1} A_e^{i-1} B_u & \dots & \sum_{i=1}^{n-l+1} A_e^{i-1} B_u \end{array} \right]_{n \times l}$

Finally,  $Y_n(k+1|k)$  can be optimized by modulating  $\Delta P(k)$ .

### 2.2. Frequency Departs from Nominal Value

When the frequency departs from its nominal value, the control objective response to the frequency change,  $\omega$  changed little ( $\omega \approx 0$ ). Set the frequency deviation  $\omega_{depart}$  as

$$\omega_{depart}(i) = \omega(i) - \omega(i-1) \quad (i = k, k+1, \dots, k+n-1) \quad (7)$$

Thus, the discrete model for  $\omega_{depart}$  can be represented as

$$\begin{cases} \Delta \omega_{depart}(i) = \Delta \omega(i) \\ \omega_{depart}(i+1) = \Delta \omega(i+1) + \omega_{depart}(i) \end{cases} \quad (8)$$

Also, output process  $Y_{depart}(i+1|i)$  associated with  $\omega_{depart}$  can be represented as

$$Y_{depart}(i+1|i) = I\omega_{depart}(i) + S_x \Delta \omega(i) + S_u \Delta P(i) + S_e \Delta P_{OUT}(i) \quad (9)$$

$\omega_{depart}(k) = 0$  when  $i = k$  is clear. Then, the optimized cost function with  $\omega_{depart}$  can be represented as

$$G_{depart} = \min \left\{ \|\Sigma_{depart} [Y_{depart}(k+1|k) - Y_{desire}(k+1)]\|^2 + \|\Sigma_1 \Delta P(k)\|^2 \right\} \quad (10)$$

where  $\Sigma_{depart} = \text{diag}(\lambda_D, \lambda_D, \dots, \lambda_D)$ ,  $\Sigma_1 = \text{diag}(\lambda_1, \lambda_1, \dots, \lambda_1)$

$\lambda_D$  and  $\lambda_1$  are weighting factors for frequency and power augmentation when frequency departs from the nominal. Desired steady state  $\omega_{desire}$  is zero. So, reference output is

$$Y_{desire}(k+1) = [0 \ 0 \ \dots \ 0]^T$$

Also, cost function (10) results in a quadratic programming problem. Introduce the intermediate variable  $\tau$ :

$$\tau = \left\{ \begin{array}{l} \left[ \Sigma_{depart} (Y_{depart}(k+1) - Y_{desire}(k+1)) \right] \\ \Sigma_1 \Delta P(k) \end{array} \right\} \quad (11)$$

$$= \left[ \begin{array}{c} \Sigma_{depart} S_u \\ \Sigma_1 \end{array} \right] \Delta P(k) - \left[ \begin{array}{c} \Sigma_{depart} E_{depart}(k+1|k) \\ 0 \end{array} \right] = Ax - b$$

where  $E_{depart}(k+1|k) = Y_{desire}(k+1) - S_x \Delta \omega(k) - S_e \Delta P_{OUT}$

By using a quadratic cost function, the MPC cost function can be written simply with equal weights as a cost function  $G_{depart}$ :

$$G_{depart} = \min(\tau^T \tau) = \min[(Ax - b)^T (Ax - b)] \quad (12)$$

The aim is then to minimize departure from nominal frequency over a brief look-ahead period. It is straightforward to see that  $G_{depart}$  optimized when

$$\begin{cases} 2A^T(Ax - b) = 0 \\ 2A^T A > 0 \end{cases} \quad (13)$$

Substituting (11) into (13), the algebraic simplification yields the optimized  $\Delta P^*(k)|_{depart}$  as

$$\Delta P^*(k)|_{depart} = (S_u^T \Sigma_d^T \Sigma_d S_u + \Sigma_1^T \Sigma_1)^{-1} S_u^T \Sigma_d^T \Sigma_d E_{depart}(k+1|k) \quad (14)$$

### 2.3. Frequency Recovery to Nominal Value

For the frequency recovery to the nominal value, the control objective is to accelerate the frequency dynamics to return the frequency to normal, which entails that  $\omega$  changes quickly. Define the recovery difference as

$$\omega_{recover}(i) = \omega(i) - \omega_{REF}(i = k, k+1, \dots, n) \quad (15)$$

where  $\omega_{REF}$  is calculated via droop control which is the steady state post-disturbance value.

A discrete model for  $\omega_{recover}$  can be obtained as

$$\begin{cases} \Delta \omega_{recover}(i) = \Delta \omega(i) \\ \omega_{recover}(i+1) = \Delta \omega(i+1) + \omega_{recover}(i) \end{cases} \quad (16)$$

Also, the output process  $Y_{recover}(i+1|k)$  is seen to be:

$$Y_{recover}(i+1|k) = I\omega_R(i) + S_x \Delta \omega(i) + S_u \Delta P(i) + S_e \Delta P_{OUT}(i) \quad (17)$$

The optimized cost function for  $\omega_{recover}$  is

$$G_{recover} = \min \left\{ \|\Sigma_{recover} [Y_{recover}(k+1|k) - Y_{desire}(k+1)]\|^2 + \|\Sigma_2 \Delta P(k)\|^2 \right\} \quad (18)$$

where  $\Sigma_{recover} = \text{diag}(\lambda_R, \lambda_R, \dots, \lambda_R)$ ,  $\Sigma_2 = \text{diag}(\lambda_2, \lambda_2, \dots, \lambda_2)$

$\lambda_R$  and  $\lambda_2$  are weighting factors for frequency and power augmentation when frequency recovers to the nominal. The desired steady state  $\omega_{recover}$  is 0, and the reference output is

$$Y_{desire}(k+1) = [0 \ 0 \ \dots \ 0]^T$$

The quantity  $G_{recover}$  can be optimized by simple optimization, and optimization of  $\Delta P^*(k)|_{recover}$  for  $G_{recover}$  can be represented as

$$\Delta P^*(k)|_{recover} = (S_u^T \Sigma_r^T \Sigma_r S_u + \Sigma_2^T \Sigma_2)^{-1} S_u^T \Sigma_r^T \Sigma_r E_{recover}(k+1|k) \quad (19)$$

where  $E_{recover}(k+1|k) = -I\omega_R(k) + Y_R(k+1) - S_x \Delta \omega(k) - S_e \Delta P_{OUT}(k)$

### 3. Centralized Control of Frequency

We regard the fast inverter dynamics of distributed generation as a cost of VSC's voltage vector set point changes, and dynamics of the stored energy level of battery energy storage systems (BESSs) as a cost of energy storage's status of charge, cost of bus voltage from its reference set point, and cost of tie line bus in the proposed centralized MPC. This paper mainly accomplishes the secondary frequency control (SFC) and minimization of the operational cost of the proposed power systems during the power flow optimization is reflected on tertiary frequency control. This is the reason why we use MPC for the FFC which can take full advantage of different inverter-based devices such as inverter and VSC. The power flow optimization only considers a steady-state optimization. Goal function is to minimize the cost of VSC's voltage vector set point change, cost of battery energy storage status of charge (SOC), cost for the deviation of voltage from its reference set point ( $V_{ik}$ ), and cost for the deviation of the net tie-line active power. Centralized controller determines the power output of each converter to take part in fast frequency control. The goal function's purpose is to minimize the total control effort over the full horizon  $k \in K$  and over all devices units  $i$  (34a). ROCOF is computed for all generators in (34b), equality constraint each individual VSC's charging power in (34c), frequency limit in (34i), and SOC in equation (34d). Active and reactive power generated by the bus in the distributed generation deduct load are represented with the (34e) and (34f). Active power of net power tie-line is in (34g). VSC's charging and discharging active power limit, and battery energy storage system SOC limit are in (34h). Distributed generation (DG) active and reactive power limit, and bus  $V_{ik}$  deviation from its reference set points are in (34j). All these equality and inequality constraints are required for the fast frequency control within the IEEE 39-bus.

$$\min_{k \in K} \sum_{i \in N^G} \left( \sum_{i \in N^G} C_{P_{ik}}^{VSC} \|\Delta P_{ci}^*(k)\| + \sum_{i \in N^{ES}} C_{ik}^{BESS} + \sum_{i \in N} C_{ik}^V + \sum_{s \in S} C_{sk}^{TIE} \right) \quad (34a)$$

$$\frac{d}{dt} f_j(k) = \frac{f_j(k+1) - f_j(k)}{T_s} \quad (34b)$$

$$P_{ci}(k) = P_{ci}^* + \sum_{l=1}^k \Delta P_{ci}^*(l) + R_{ci}^P (\omega_{ci}^* - \omega_{ci}(k)) \quad (34c)$$

$$SOC_{ik} = SOC_{i(k-1)} + (\eta_{ci} P_{cik} - \eta_{di}^{-1} P_{dik}) T \quad (34d)$$

$$P_{Gik} - P_{cik} + P_{dik} - P_{Lik} = P_i^C + \sum_{j \in \{i\} \cup N_i} (A_{ij} \Delta V_{jk} + B_{ij} \Delta \theta_{jk}) \quad (34e)$$

$$Q_{Gik} - Q_{Lik} = Q_i^C + \sum_{j \in \{i\} \cup N_i} (C_{ij} \Delta V_{jk} + D_{ij} \Delta \theta_{jk}) \quad (34f)$$

$$P_{sk}^{TIE} = \sum_{(i,j) \in L_s} (P_{ij}^C + E_{ij}^j \Delta V_{jk} + F_{ij}^j \Delta \theta_{jk} + Y_{ij}^i \Delta V_{ik} + Z_{ij}^i \Delta \theta_{ik}) \quad (34g)$$

$$0 \leq P_{cik}(k) \leq \bar{P}_{ci}, 0 \leq P_{dik}(k) \leq \bar{P}_{di}, \underline{SOC}_i \leq SOC_{ik} \leq \overline{SOC}_i \quad (34h)$$

$$\underline{f} \leq f_i(k) + R_{ci}^P \Delta P_{ci}^*(k) \leq \bar{f} \tag{34i}$$

$$0 \leq P_{Gik} \leq \bar{P}_{Gi}, \quad 0 \leq Q_{Gik} \leq \bar{Q}_{Gi}, \quad \underline{V}_i \leq V_{ik} \leq \bar{V}_i \tag{34j}$$

#### 4. Model Testing and Control Fulfillment

The suggested FFC methods carried out and tested on the IEEE 39-bus system as shown in Fig. 2. This is a popular 10-machine representation of the New England power system with generator at node 10-machine depiction of the New England power system with generator at node 10 meaning the collection of a large number of generators. Inverter based generation is placed at nodes 1, 2, and 3. The red symbol which represents disturbance location. The pertinent load and generation parameters can be found in [13], [14]. The simulations have been accomplished in MATLAB which includes detailed representation of generator and transmission line dynamics [19]. The examined system consists of seven conventional generators, and three synchronous generators from the initial system exactly at nodes 1, 2, and 3, have been displaced by converter interfaced units of 1000 MW installed power and 10 MWh battery energy storage system. The individual power ratings and output limits of the stay behind synchronous generators have been conserved. All VSCs perform in grid forming mode and are provided with the fast frequency control layer.

The disturbances are produced by step changes in active power at network buses of engaged, therefore imitating either a loss of load or a loss of generator. The first stage of automatic load shedding is established in the case of frequency variation beyond  $\pm 0.5 \text{ Hz}$ , although the ROCOF protection is activated at  $\pm 1 \text{ Hz/s}$  for the ROCOF estimations mean value over a  $240 \text{ ms}$  cycle. Thus, the frequency related threshold values are established as follows (34):  $\bar{f}_{lim} = 60.5 \text{ Hz}$ ,  $\underline{f}_{lim} = 59.5 \text{ Hz}$ ,  $\dot{\bar{f}}_{lim} = \frac{1 \text{ Hz}}{s}$ ,  $\dot{\underline{f}}_{lim} = -\frac{1 \text{ Hz}}{s}$ . The battery energy storage system SOC and VSC power output are defined in per unit, and the maximum and minimum limits are established to 1 and 0, respectively.

The prediction horizon of the MPC based controller is set to three-time steps with a sampling period of  $240 \text{ ms}$ . On the other hand, the prediction horizon length of  $720 \text{ ms}$  considers a trade-off between computational effort and controller performance. The MPC sampling period is decided as it surpasses all delays related with the supervisory layer and converter, also the time required to compute the optimal control decisions. The real-time ROCOF measures  $\dot{\omega}_{max}$  necessary for the computation of the disturbance magnitude  $\Delta P$  is attained from averaging the internal ROCOF state signal  $\dot{\omega}$  over a time interval of  $12 \text{ ms}$  in the instant consequence of a disturbance.

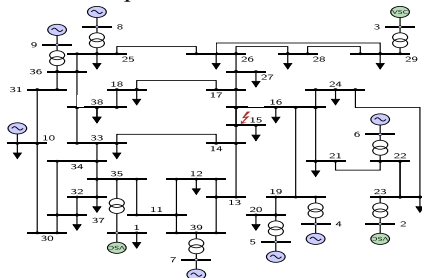


Figure 2. IEEE 39-bus test system.

### 4.1. Simulation of Frequency Control Performance

Centralized grid controller acquires an errorless disturbance estimate across the independent of disturbance location, wide area measuring, and consequently with low error. The values of estimated and practical disturbance magnitudes for each reflected on bus and every VSC are showed in Table I. Let us reflect on a power disturbance of 1500 MW at node 15 with 720 ms. Fig. 3 demonstrate frequencies, active and reactive power outputs of separate generators for FFC methods. The VSC at node 3 stay behind inactive because of the large electrical distance to the disturbance location and resulting underestimation of the disturbance. Nonetheless, the assistance from the other two converters is enough to pay off the disturbance and inhibit load shedding. However, the global MPC based grid controller transmits all three units equally, with the exactly alike total control expenditure is for MPC methods. Generally, lower control effort is taken on in the centralized approach. ROCOF is within the critical set points, active and reactive power is increased after the frequency disturbance based on the VSC’s location points. Due to non-weighting MPC methods, VSC generations are well operated with the connection of VSC bus 1 and VSC bus 2 within the disturbances.

**Table 1.** Fault case at bus with applied disturbance size and estimated asymmetry for each VSC

Bus	Disturbance [MW]	Estimated disturbance [MW]		
		VSC 1	VSC 2	VSC 3
15	1550	1505	1900	825

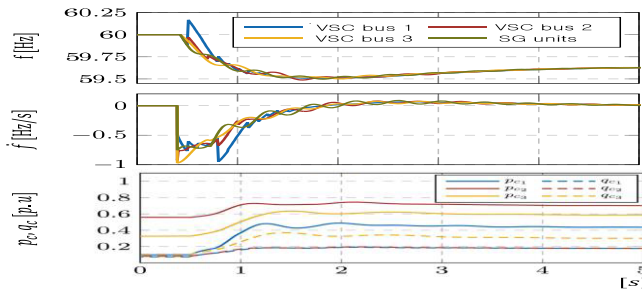


**Figure 3.** Centralized control individual frequency, frequency change at unit time, active and reactive power output for FFC proposed method following a disturbance at bus 15.

### 4.2. DC Side Dynamics Analysis

The most pertinent variables explaining the dynamics of the DC side circuit, especially the inverter neutral point voltage ( $U_{NPV}$ ), and the energy storage system SOC ( $U_{dc}$ ) are depicted in Fig. 4 for individual VSC units and disturbance at bus 15. The set-up energy capacity of the batteries is presumed to be 10 MWh, with the initial BESS’s SOC set to 0.5 p.u. The disturbance and the inverter setting value adjusts due to power imbalances at the capacitor node, bring about DC voltage plunge which are rapidly fixed up by the DC side controls using available energy of the battery. In the end, the input DC voltage indicates faster dynamics compared to the output power, which could potentially bring about high current injections. From Fig. 4, the first graph shows, BESS’s DC side voltage is set to 0.5 SOC; thus, it is controlled within 0.5 SOC even if there is the disturbance. During the control period, neutral point voltage of DC side is effectively controlled with

the disturbance. The second graph tells, inverter's DC side is controlled within the little bit over than 0.05 p.u. voltage difference.

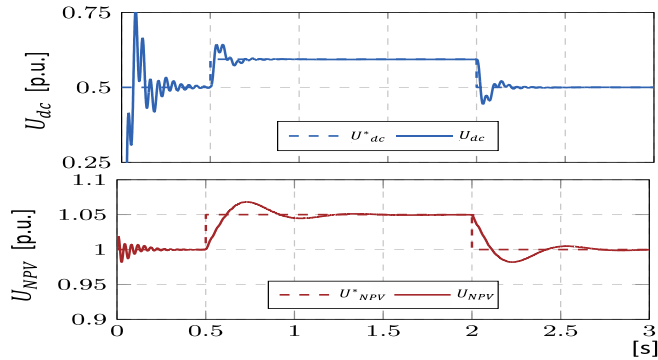


**Figure 4.** Overall maintenance of BESS  $U_{dc}$ , and overall maintenance of BESS  $U_{NPV}$  voltage reaction for proposed method following a disturbance at bus 15.

## 5. Conclusion

This paper proposes a novel FFC approach for optimization of MPC based inverters interfaced DGs in low inertia systems, which take advantage of their agile response to prevent frequency shedding cases. A loop of MPC based supervisory control layer is added to the control scheme not to make weighting factor with NPC inverter control approach. In reaction to a large disturbance, system controls the converter setting value to hold the frequency within decided set bounds. Centralized control method was considered and proven to be effective which can be implemented without fast communication framework via enhancement in fast frequency prediction accuracy with inverters. For future works, it is necessary to build detailed VSC with the model predictive control within the centralized frequency control for the fast frequency control within IEEE 39-bus system.

## References

- [1] D. Gautam, L. Goel, R. Ayyanar, V. Vittal, and T. Harbour. Control strategy to mitigate the impact of reduced inertia due to doubly fed induction generators on large power systems. *IEEE Trans. Power Systems*, 2010 Jul; 26(1):214-10.
- [2] Q. Hong, M. Norris, I. Abdulhadi, M. Karimi, V. Trezija, B. Marshall, K. Bell, and C. Booth. Fast frequency response for effective frequency control in power systems with low inertia. *The Journal of Engineering*, 2019 Mar; 2019(1):1696-6.
- [3] Q. C. Zhong, and G. Weiss. Synchronverters: Inverters that mimic synchronous generators. *IEEE Trans. Ind. Electron.*, 2011 Apr; 58(4):1259-8.
- [4] T. Vandoorn, B. Meersman, J. Kooning, and L. Vandevelde. Transition from islanded to grid-connected mode of microgrids with voltage-based droop control. *IEEE Trans. Power Systems*, 2013 Aug; 28(3): 2545-9.
- [5] D. Bazargan, B. Bahrani, and S. Filizadeh. Reduced capacitance battery storage DC-link voltage regulation and dynamic improvement using a feedforward control strategy. *IEEE Trans. Energy Conversion*, 2018 Nov; 33(4):1659-10.
- [6] J. B. Rawlings, D. Q. Mayne, and M. Diehl. *Model Predictive Control: Theory, Computation, and Design*. Madison: Nob Hill, 2017. 112 p.

- [7] A. M. Ersdal, L. Imsland, and K. Uhlen. Model predictive load-frequency control. *IEEE Trans. Power Syst.*, 2016 Jan; 31(1):777-9.
- [8] A. N. Venkat, I. A. Hiskens, J. B. Rawlings, and S. J. Wright, editors. Distributed output feedback MPC for power system control. *Proc. 45<sup>th</sup> IEEE Conf. Decis. Control*; 2006 Dec. 4038 p.
- [9] T. Zhang, and H. B. Gooi, editors. Hierarchical MPC-based energy management and frequency regulation participation of virtual power. *Proc. IEEE PES Innovative Smart Grid Technologies*; 2014 Oct 1p.
- [10] A. Ulbig, T. Rinke, S. Chatzivasileiadis, and G. Andersson, editors. Predictive control for real-time frequency regulation and rotational inertia provision in power systems. *Proc. 52nd IEEE Conf. Decis. Control*, 2013 Dec. 2946 p.
- [11] L. Papangelis, M.-S. Debry, T. Prevost, P. Panciatici, and T. V. Cutsem. Decentralized model predictive control of voltage source converters for AC frequency containment. *Int. J. Elect. Power Energy Syst.*, 2018 Jan; 98(1): 342-8.
- [12] A. Fuchs, M. Imhof, T. Demiray, and M. Morari. Stabilization of large power systems using VSCHVDC and model predictive control. *IEEE Trans. Power Del.*, 2014 Feb;29(1): 480-8.
- [13] T. Athay, R. Podmore, and S. Virmani. A practical method for the direct analysis of transient stability. *IEEE Trans. Power App. Syst.*, 1979 Mar;98(2):573-12.
- [14] M. A. Pai. *Energy Function Analysis for Power System Stability*. Berlin, Germany: Springer-Verlag, 1989. 145 p.
- [15] J. A. Short, D. G. Infield, and L. L. Freris. Stabilization of grid frequency through dynamic demand control. *IEEE Trans. Power Sys.*, 2007 Jul;22(3): 1284-12.